BIOCHEMISTRY
including biophysical chemistry & molecular biology

Article

pubs.acs.org/biochemistry

Exploring the Catalytic Mechanism of Alkanesulfonate Monooxygenase Using Molecular Dynamics

Kira Armacost, Jonathan Musila, Symon Gathiaka, Holly R. Ellis,* and Orlando Acevedo*

Department of Chemistry and Biochemistry, Auburn University, Auburn, Alabama 36849, United States

Supporting Information

ABSTRACT: The complex mechanistic properties of alkanesulfonate monooxygenase (SsuD) provide a particular challenge for identifying catalytically relevant amino acids. In response, a joint computational and experimental study was conducted to further elucidate the SsuD mechanism. Extensive unbiased molecular dynamics (MD) simulations were performed for six SsuD systems: (1) substrate-free, (2) bound with $FMNH_2$, (3) bound with a C4a-peroxyflavin intermediate ($FMNOO^-$), (4) bound with octanesulfonate (OCS), (5) co-bound with $FMNH_2$ and OCS, and (6) co-bound with $FMNOO^-$ and OCS. A previous theoretical study suggested that salt bridges between Arg297 and Glu20 or Asp111 initiated conformational changes critical for catalysis. However, our MD simulations and steady-state kinetic experiments did not corroborate this result. Similar k_{cat}/K_m values for both the E20A and D111A SsuD variants to wild-type SsuD suggest that the salt bridges are not critical to the desulfonation mechanism. Instead, the predicted role of Arg297 is to favorably interact with the phosphate group of the reduced flavin. Concomitantly, Arg226 functioned as a "protection" group shielding $FMNOO^-$ from bulk solvent and was more pronounced when both $FMNOO^-$ and OCS were bound. The stabilization of $FMNOO^-$ through electrostatic interactions with Arg226 would properly position the C4a peroxy group for the proposed nucleophilic attack on the sulfur of octanesulfonate.

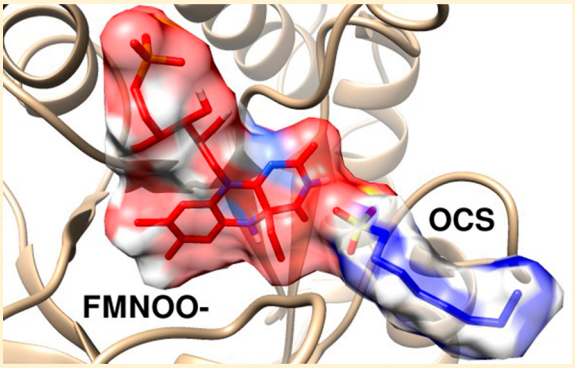

Alkanesulfonate monooxygenase (SsuD) is a flavin-dependent enzyme responsible for sulfite production in bacterial organisms during times of limited sulfur availability.[1−8] Reduced flavin and dioxygen are utilized by SsuD to generate a C4a-(hydro)peroxyflavin intermediate that is directly responsible for carbon−sulfur bond cleavage of 1-alkanesulfonates, generating the sulfite product and corresponding aldehyde (Scheme 1).[3,5,6,9] As part of a two-component system, a flavin reductase (SsuE) provides $FMNH_2$ by catalyzing the reduction of FMN with reducing equivalents provided by NADPH. The higher affinity of SsuD for reduced flavin emphasizes that the SsuD active site environment is dependent upon which redox form of the flavin is bound to the enzyme.[3,5,6,9,10]

Scheme 1. Two-Component Flavin-Dependent Monooxygenase System

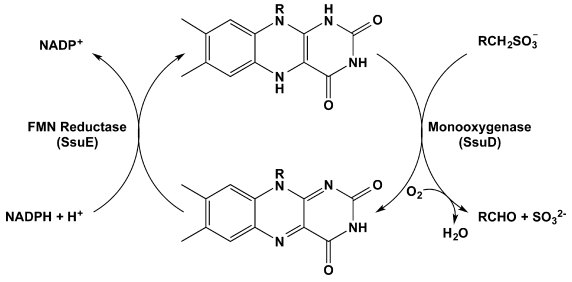

On the basis of structural similarities, the SsuD enzyme belongs to the bacterial luciferase family, which includes bacterial luciferase and long-chain alkane monooxygenase (LadA).[7,11,12] All members of this family form a triosephosphate isomerase (TIM)-barrel fold but vary from canonical TIM-barrel structures by the presence of several insertion regions. One insertion region present in SsuD (Glu233−Asp307) contains a largely unresolved loop, suggesting conformational mobility.[7] This disordered region lies near the putative active site at the C-terminal end of the β-barrel and is highly conserved in all SsuD homologues. While SsuD variants containing partial deletions of this loop region can bind reduced flavin and exhibit no gross changes in secondary structure relative to that of wild-type SsuD, they are catalytically inactive.[13] Consequently, the loop has been proposed to undergo a lid gating conformational change following the binding of substrate(s) in SsuD as a means of protecting the flavin intermediates from bulk solvent and potentially mediating the transfer of $FMNH_2$ from SsuE to SsuD.[5,14] In addition, it was previously demonstrated that octanesulfonate

Received: February 18, 2014
Revised: April 30, 2014
Published: May 5, 2014

dx.doi.org/10.1021/bi5002085 | *Biochemistry* 2014, 53, 3308−3317

could not bind to SsuD unless reduced flavin was bound first. Therefore, the mechanism of SsuD is dependent on the reduced flavin binding prior to the alkanesulfonate substrate. These results suggest an $FMNH_2$-induced conformational change is essential to allow octanesulfonate to bind.[4,5]

A conserved arginine residue (Arg297) located in the mobile loop insertion sequence significantly contributes to catalysis, as well, as the R297C and R297A SsuD variants yielded no observed activity and the R297K variant substantially lowered the k_{cat}/K_m value relative to that of wild type.[3,7] Interestingly, the Arg297 residue is positioned away from the active site and would have to undergo a conformational change to be catalytically relevant.[7] Computational studies have proposed that conformational changes that alter active site accessibility are driven by salt bridge formation involving Arg297 and Glu20 or Asp111.[15]

It has been demonstrated that SsuD forms a C4a-(hydro)-peroxyflavin intermediate in the absence of octanesulfonate and at low octanesulfonate concentrations, but the nature of the flavin peroxide has not been determined.[5] Therefore, catalysis by SsuD could occur through a C4a-hydroperoxyflavin (FMNOOH) or C4a-peroxyflavin ($FMNOO^-$) intermediate.[2] For the mechanism involving a C4a-hydroperoxyflavin, an active site base is proposed to abstract a proton from C1 of the alkanesulfonate to generate a carbanion intermediate. The carbanion intermediate makes a nucleophilic attack on the hydroperoxyflavin to generate an unstable 1-hydroxyalkanesulfonate that decomposes to the corresponding aldehyde and sulfite. On the basis of the mechanism of other flavin monooxygenases, the C4a-peroxyflavin ($FMNOO^-$) would seem to be the most likely intermediate in the reaction making a nucleophilic attack on the sulfonate functional group to form an initial alkanesulfonate peroxyflavin intermediate (Scheme 2).

Scheme 2. Proposed Chemical Mechanism of SsuD after All Substrates Have Been Bound and O_2 Has Been Activated

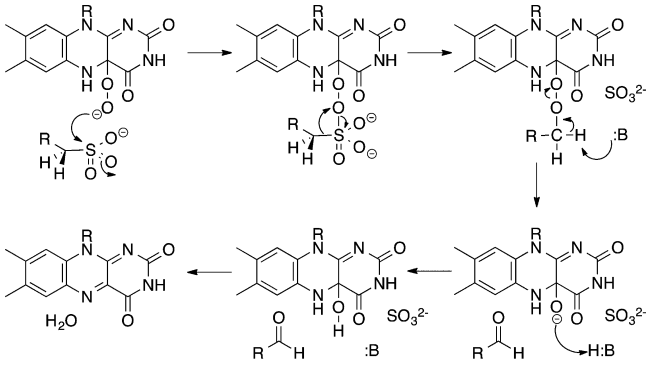

A Baeyer–Villiger rearrangement of the flavin adduct would release the sulfite product and generate a peroxyalkane intermediate. Because of the unique carbon–sulfur bond cleavage step catalyzed by SsuD, elucidating the mechanistic properties of SsuD has proven to be a considerable challenge despite extensive research efforts.[2,3,5,16] Identifying the specific residues that directly participate in the oxygenolytic cleavage of alkanesulfonate has been particularly difficult. For example, modification of the sole cysteine residue (Cys54) with methylmercury resulted in the inactivation of SsuD. Further kinetic analysis implicated Cys54 in the stabilization of the C4a-(hydro)peroxyflavin intermediate, potentially lowering the pK_a of the putative active site acid.[4,17] A highly conserved active site residue, His228, was proposed to be the catalytic base responsible for abstraction of the proton from the alkanesulfonate peroxyflavin adduct (Scheme 2).[7,8,11,12,18–21] Kinetic characterization of His228 SsuD variants contested the catalytic role of this residue, and two more potential active site bases (His11 and His333) were also eliminated from consideration.[16] While the specific active site residue behaving as the base is unclear, previous studies support Arg226 as the active site acid participating in the protonation of the $FMNO^-$ intermediate in the proposed Baeyer–Villiger mechanism (Scheme 2).[16] Conserved arginine residues are often critical in Baeyer–Villiger flavin monooxygenases in stabilizing the peroxyflavin intermediate.[22–24] Variants of Arg226 possessed no detectable activity, and there was no measurable formation of the C4a-(hydro)peroxyflavin intermediate even though the affinity for reduced flavin was similar to that of wild type.[16]

To further investigate the roles of the conserved Arg residues and mobile loop in the proposed mechanism and potential substrate-induced conformational changes in SsuD, unbiased molecular dynamics (MD) simulations were performed at atomic resolution for six SsuD forms: (1) substrate-free, (2) bound with $FMNH_2$, (3) bound with the C4a-peroxyflavin intermediate ($FMNOO^-$), (4) bound with octanesulfonate (OCS), (5) co-bound with $FMNH_2$ and OCS, and (6) co-bound with $FMNOO^-$ and OCS. Homology modeling was used to insert unresolved residues 250–282 into the mechanistically important loop region. A total simulation time of 2.1 μs was completed in this study. Extensive analysis has been conducted for conserved amino acid residues located within the active site and on the mobile loop region. In addition, experimental steady-state kinetic analyses and FMN binding studies have been performed to support the theories derived from the calculations. This joint computational and experimental study further clarifies the role of protein dynamics in the binding of substrates and provides additional insight into the catalytic mechanism of sulfite production in SsuD.

EXPERIMENTAL PROCEDURES

Enzyme Preparation. Initial Cartesian coordinates for the SsuD systems were generated from a 2.3 Å resolution crystal structure [Protein Data Bank (PDB) entry 1M41].[7] The reported structure contains residues 1–249 and 283–361 per monomer, as no clear density was available for internal residues 250–282 or C-terminal residues 362–380. Residues 250–282 were constructed (Figure 1) using a comparative modeling program, MODELLER version 9.10.[25] The program generated a refined three-dimensional model of the given protein sequence (target) based primarily on its alignment with one or more proteins of known structure (templates). The templates used were the SsuD structure (PDB entry 1NQK) and the structure of the luciferase-like monooxygenase from *Bacillus cereus* (PDB entry 3RAO). The $FMNH_2$ ligand was inserted into the active site region of SsuD based on a superposition with coordinates from a LadA enzyme with a bound FMN (PDB entry 3B9O).[12] Recent studies have suggested that conserved residues among the flavin-dependent monooxygenases are structurally related and possess similar catalytic activities and should therefore provide a reasonable starting point for the simulations.[3,4]

AutoDock Vina. Inserting octanesulfonate into SsuD was performed using AutoDock Vina.[26] A grid box was fit to cover the proposed active site (Table S1 of the Supporting Information), where 10–20 binding modes were analyzed to

dx.doi.org/10.1021/bi5002085 | *Biochemistry* 2014, 53, 3308–3317

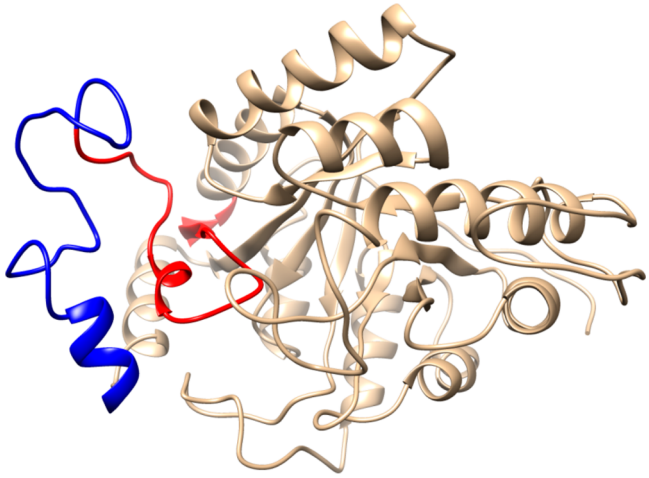

Figure 1. Apo SsuD structure highlighting the mobile loop (red and blue) where the modeled-in residues (250−282) are colored blue.

determine the most probable structure based on previously proposed catalytic sites.[3,4,7] Standard flexible protocols of AutoDock Vina using the Iterated Local Search global optimizer algorithm were employed to evaluate the binding affinities of the molecule and interactions with the receptors. All active site residues, as defined by the box size used for the receptors, were set to be rotatable. Calculations were conducted with the exhaustiveness of the global search set to 100, the number of generated binding modes set to 20, and the maximal energy difference between the best and worst binding modes set to 5.

MD Protocol. MD simulations were performed on SsuD with six different combinations of substrates. In each case, SsuD was simulated as a monomer. The resulting structures were fed into the leap module of the AMBER 12 package where the appropriate hydrogen atoms were added.[27] The enzyme was solvated in a box of explicit TIP3P water molecules[28] extending at least 10 Å beyond the enzyme, and sodium ions were added to maintain charge neutrality. The ff99SB force field[29] was used to construct the topology files for the protein, while the parameters for the ligands were obtained from the generalized AMBER force field (GAFF).[30] Each ligand was optimized by conducting a Monte Carlo conformational search using the BOSS program[31] and the OPLS force field.[32] The five lowest-energy structures were reoptimized at the MP2/6-31G(d) theory level using Gaussian 09 software,[33] and the lowest-energy MP2 structure was used to determine the restrained electrostatic potential (RESP) partial atomic charges using HF/6-31G(d) and the AmberTools antechamber module.

For each system, the initial structure was conjugate gradient (CG) minimized for 200 steps for the water molecules only, followed by 10000 steps of CG optimization of the entire system to remove any bad contacts. After minimization, the full system was gradually heated from 0 to 300 K using a constant *NVT* ensemble for 50 ps of MD using the weak-coupling algorithm with a temperature coupling value of 2.8 ps. The system was then switched to a constant *NPT* ensemble at 300 K and 1 atm using a coupling value of 2.0 ps for both temperature and pressure and run for 500 ps. Finally, the system was returned to *NVT* and equilibrated for an additional 500 ps. Following equilibration, 300 ns of production data was collected at constant *NVT* for each protein complex using the GPU-accelerated version of AMBER 12.[34] To verify that the GPU-based simulations yielded reasonable results, a shorter simulation of 10 ns was conducted using the CPU AMBER version to check the Ewald error estimate and to ensure a stable system. All MD simulations utilized the particle mesh Ewald method to compute the long-range Coulomb force, periodic boundary conditions with a nonbonded cutoff distance of 12 Å, and a time step of 1.0 fs.[35] All calculations were conducted on computers located at the Alabama Supercomputer Center and Auburn University.

Analysis. The major conformational changes of the SsuD enzyme were modeled with root-mean-square fluctuations (rmsfs), which calculate the positional deviations of the SsuD enzyme relative to a reference structure. The trajectories required for Bio3D were made using VMD.[36] Clustering, hydrogen bond analysis, distance calculations, and root-mean-square deviation (rmsd) calculations were conducted using the ptraj and cpptraj programs within AmberTools.[37] For the clustering calculations, the average linkage algorithm was utilized.[38] All enzyme figures were made using Chimera.[39]

Construction of SsuD Variants. The recombinant pET21a plasmid containing the *ssuD* gene was used to construct the SsuD variants. The GAA codon for Glu20 and the GAT codon for Asp111 were substituted with Ala codon GCG. Confirmation of the resultant SsuD variants was performed by DNA sequence analysis at Davis Sequencing (University of California, Davis, CA). Confirmed variants were transformed into *Escherichia coli* BL21(DE3) competent cells for protein expression, and glycerol stocks of wild-type SsuD and its variants were stored at −80 °C. Each SsuD variant was purified as previously reported.[10] Following purification, stocks of the variant and wild-type SsuD enzymes were stored in 25 mM potassium phosphate buffer (pH 7.5), 100 mM NaCl, and 10% glycerol at −80 °C. The enzyme concentrations were determined spectrophotometrically by using an absorption coefficient of 47900 M^{-1} cm^{-1} at 280 nm. Wild-type SsuE was expressed and purified as previously described and the concentration determined spectrophotometrically by using an absorption coefficient of 20340 M^{-1} cm^{-1} at 280 nm.[10]

Table 1. Dominant Clusters for the Apo and Bound SsuD Systems[a]

enzyme	cluster	% occupied	no. of frames	time window (ns)	average rmsd (Å)
apo	6	25.4	15212	104−152	3.78
$FMNH_2$	9	36.2	21717	195−300	4.96
$FMNOO^-$	3	34.2	20499	23−127	4.29
OCS	8	43.4	26059	97−231	5.91
$FMNH_2$ and OCS	9	65.6	39340	102−300	4.34
$FMNOO^-$ and OCS	3	37.5	22476	44−163	3.98

[a]The rmsds are the average values over the range over which each cluster occurs.

dx.doi.org/10.1021/bi5002085 | *Biochemistry* 2014, 53, 3308−3317

Steady-State Kinetic Analyses and FMN Binding. Steady-state kinetic measurements were performed for E20A, D111A, and wild-type SsuD as previously described.[5] Oxidized flavin binding was assessed for E20A, D111A, and wild-type SsuD using fluorimetric titration of the SsuD enzymes with oxidized flavin. Spectra were recorded on a Cary Eclipse Agilent fluorescence spectrophotometer with an excitation wavelength of 280 nm and emission intensity measurements at 344 nm. Titration of SsuD was performed by the addition of FMN aliquots (2.6−104 μM) to a 1.0 mL solution of 0.5 μM SsuD in 25 mM potassium phosphate (pH 7.5) and 100 mM NaCl. The fluorescence spectra were recorded following a 2 min incubation after the addition of each aliquot of FMN. The concentration of bound FMN was used to calculate the K_d as previously described.[40]

RESULTS AND DISCUSSION

To identify the most dominant structural configurations for each bound and unbound SsuD system, clustering analysis was performed on every 300 ns (600000 frame) trajectory. A list of the most dominant clusters and the time occurring over their respective trajectories are listed in Table 1 and Table S2 of the Supporting Information. The second and third most dominant SsuD structures from each simulation are illustrated in the Supporting Information (Figures S1−S6). The physical similarity of each cluster structure relative to the initial starting configuration was investigated using rmsd calculations (Figure S7 of the Supporting Information). The dominant apo cluster most closely resembled the starting structure with an average rmsd of 3.78 Å compared to values of 3.98−5.91 Å for the five other SsuD solute-bound systems (Table 1). The increasing rmsd values are consistent with the conformational changes proposed to occur after the substrates bind to the enzyme.[5,14]

Root-mean-square fluctuation (rmsf) calculations of the SsuD backbone atoms allow for a better understanding of enzyme dynamics and fluctuations in response to substrate binding. The average percent change in the rmsf for different combinations of substrate-bound SsuD compared to substrate-free SsuD is shown in Figure 2. Residues that have become more localized upon binding substrates have a positive change in rmsf, whereas residues that have become more flexible subsequent to binding have a negative change. Absolute rmsf values for all ligand−SsuD combinations are listed in the Supporting Information (Figures S8−S12). Four regions within the SsuD enzyme appear to be particularly stabilized by the binding of substrate: (a) residues 1−25, (b) residues 120−135, (c) residues 160−200, and (d) residues 280−310. Upon visual inspection of Figure 2, it is obvious that the region encompassing residues 160−200 is markedly affected by substrate binding. The residues contained within this region interact directly with the bound flavin and octanesulfonate. It is notable that the cofactor was never expelled from the binding pocket during any of the simulations. This is indicative of the induced stability of the active site region of residues 160−200 when occupied by substrates and correlates well with the conserved flavin-binding region of the LadA enzyme.[12] The region of residues 120−135 also contains active site residues that interact with the co-bound $FMNOO^-$ and OCS substrates.

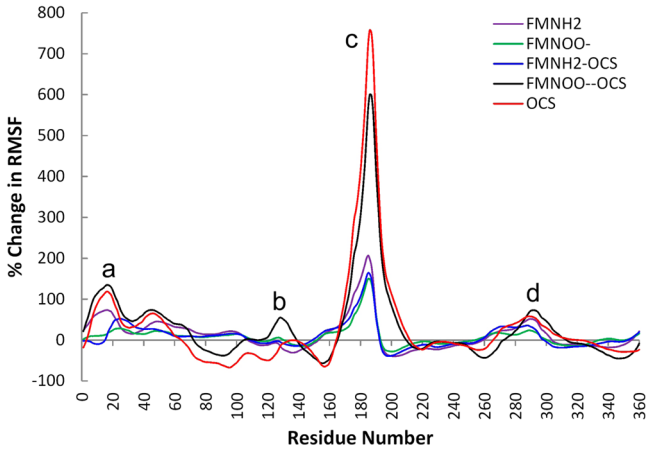

Figure 2. Average percent change in root-mean-square fluctuations (rmsfs) of the C_α backbone atoms of SsuD upon binding substrates relative to substrate-free SsuD. Enzyme regions with significant changes: (a) residues 1−25, (b) residues 120−135, (c) residues 160−200, and (d) residues 280−310. A positive change indicates residues that have become more localized upon substrate binding, and a negative change signifies enhanced fluctuations.

The other two regions (residues 1−25 and 280−310) in SsuD significantly affected by substrate binding as demonstrated by the rmsf calculations contain amino acids Glu20 and Asp297. Both residues have been associated with driving conformational changes in the active site via salt bridge formation.[15] More detail about salt bridge formation is discussed further below. Interestingly, substrate binding did not appear to influence the mobile loop region (residues 250−282). Examination of the mobile loop over multiple simulations, including two separate 300 ns simulations of the co-bound $FMNOO^-$−OCS SsuD system, did elucidate a highly active and flexible region (see the movie of the apo and $FMNOO^-$−OCS-bound SsuD systems in the Supporting Information). However, the rmsf calculations did not corroborate a substrate-induced conformational change in the mobile loop proposed to shield the reactive flavin intermediate from bulk solvent.

Previous MD calculations proposed that salt bridges between Arg297 and Asp111 or Glu20 may dictate the ability of SsuD to accept substrates into the active site.[15] The salt bridge between Arg297 and Asp111 was favored when SsuD was bound to $FMNH_2$ and would reportedly allow a "closed" conformation that could exclude further substrates or bulk solvent from entering the active site. The alternative salt bridge between Arg297 and Glu20 would occur sporadically and yield an "open" conformation allowing substrates to readily enter the pocket. The substrate-free SsuD simulations found the enzyme would frequently switch between the closed and open configurations, with no clear preference for either interaction. It should be noted that the study was performed using shorter 20 ns trajectories and lacked mobile loop residues 250−282.[15]

Our simulation of the $FMNH_2$-bound SsuD system revealed the formation of Arg297−Asp111/Glu20 salt bridges; however, distance calculations and hydrogen bond analysis indicated that they occupied <15% of the total simulation (Figures 3 and 4). Instead, Arg297 was found to behave like the conserved arginine in bacterial luciferase by forming favorable electrostatic interactions with the phosphate group of $FMNH_2$ for approximately 36% of the trajectory (Figure 5). A similar role has been proposed for Arg297 in experimental studies evaluating the potential role of this residue in catalysis.[3] Substitution of Arg297 to Ala resulted in a complete loss in activity, while the more conservative Lys substitution resulted in a 30-fold decrease in the k_{cat}/K_m values (Table 2).

dx.doi.org/10.1021/bi5002085 | Biochemistry 2014, 53, 3308−3317

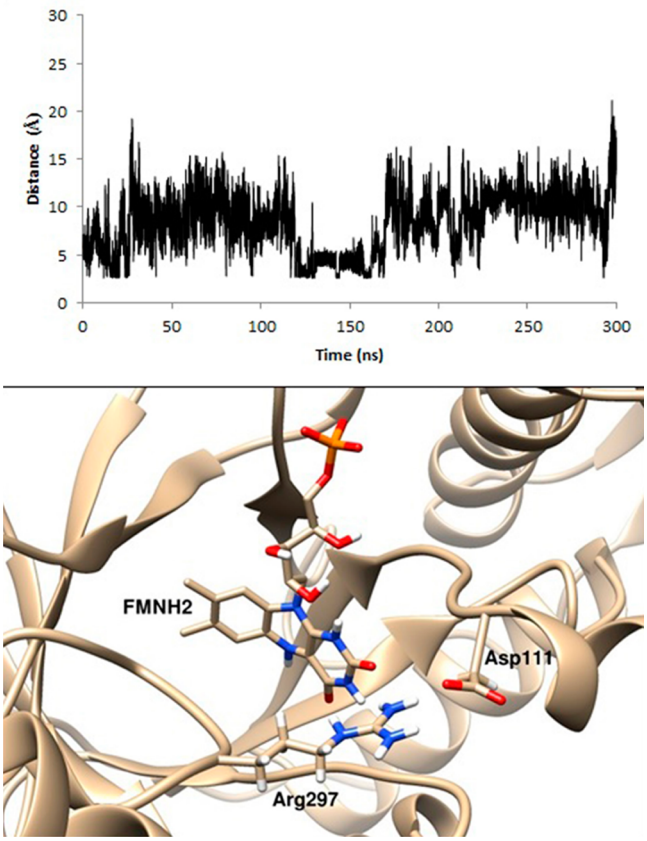

Figure 3. Distance calculation (angstroms) between Arg297 and Asp111 in SsuD when it is bound to $FMNH_2$. Illustrated structure given at 11.8 ns.

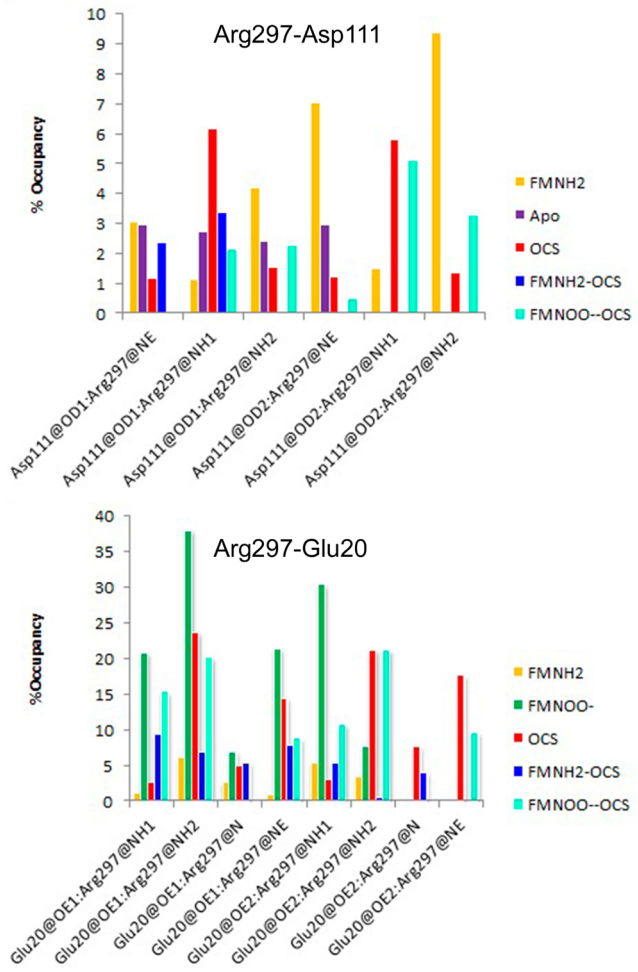

Figure 4. Hydrogen bond occupancy (acceptor:donor) between (top) Arg297 and Asp111 and (bottom) Arg297 and Glu20 for all simulations.

Interestingly, the K_d values for reduced flavin binding with the Arg297 variants were similar to that of wild-type SsuD. On the basis of the results from these studies, the proposed role of Arg297 was to stabilize the flavin through interactions with the phosphate oxygen. The interaction of Arg297 with the flavin may initiate a conformational change that favors alkanesulfonate binding and further protection of reaction intermediates. When solely bound to OCS, the Arg297−Asp111 salt bridge in SsuD was predicted to have hydrogen bond occupancies for nearly 6% of the 300 ns simulation, while the Arg297−Glu20 open conformation occurred for ∼24% of the trajectory (Figure 4). Substrate-free SsuD had approximately 3% Arg297−Asp111 hydrogen bond occupancy but essentially no Arg297−Glu20 salt bridge formation. Ultimately, the Arg297−Asp111 salt bridge proposed to "close" the active site did not have a hydrogen bond occupancy of >10% regardless of the bound substrates (Figure 4).

Intriguingly, when $FMNOO^-$ was the only ligand present in the active site, the interaction between Arg297 and the PO_4^{2-} group was significantly weakened or even nonexistent (Figure 5). In addition, the Arg297−Asp111 closed conformation occupied less than 0.1% hydrogen bonding. Arg297 is instead occupied by electrostatic interactions with Glu20 for approximately 40% of the simulation (Figure 6C). The $FMNOO^-$−OCS co-bound SsuD simulations found hydrogen bond occupancies between Arg297 and Glu20 reduced to around 20% (Figure 6D). Instead of relying upon the Arg297−Asp111 salt bridge to protect $FMNOO^-$ from solvent, Arg226 may act to stabilize the peroxy group of the flavin through electrostatic interactions. Overall, these simulations did not support the Arg297−Asp111 and Arg297−Glu20 salt bridges being relevant to catalysis.

Alanine variants of Glu20 and Asp111 were experimentally generated to evaluate the catalytic relevance of these residues through steady-state kinetic analyses. Steady-state kinetic parameters for E20A, D111A, and wild-type SsuD were obtained by monitoring the production of the TNB anion at 412 nm formed from the reaction of DTNB with the sulfite product. The k_{cat}/K_m values for the SsuD variants were similar to the wild-type value of $1.4 \pm 0.2\ \mu M^{-1}\ min^{-1}$ (Table 2). The comparable k_{cat}/K_m values suggest that the Arg297-based salt bridges are not critical to the desulfonation mechanism. In addition, there was no significant change in the K_d value for the binding of FMN by E20A and D111A SsuD relative to that of wild-type SsuD. Therefore, the dynamic conformational change to the proposed active form does not exist or is not initiated by a switch from the Arg297−Asp111 salt bridge to the Arg297−Glu20 salt bridge.

As Arg226 has been reported to play a critical role in the SsuD desulfonation mechanism, interactions have been carefully monitored between the arginine and bound substrates at different stages of the proposed Baeyer−Villiger mechanism (Scheme 2).[16] For example, Arg226 was computed to have average distances of 4−5 Å to the sulfonate group of OCS when the substrate was solely bound to SsuD. Much shorter

dx.doi.org/10.1021/bi5002085 | *Biochemistry* 2014, 53, 3308−3317

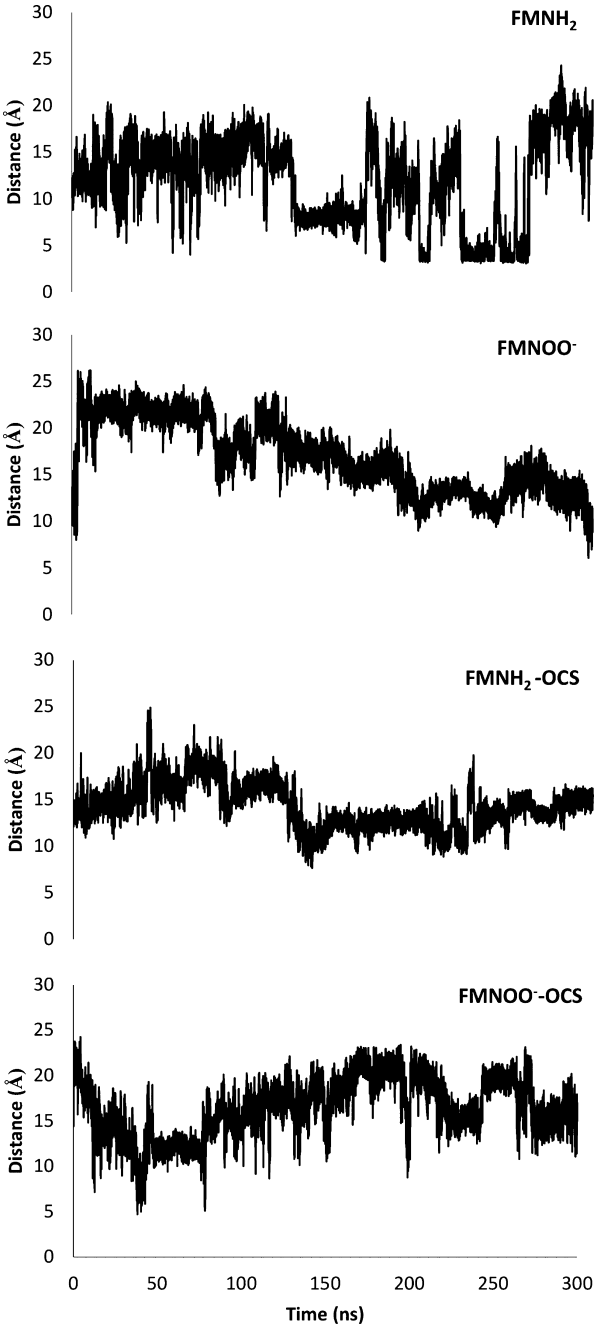

Figure 5. Distance calculations (angstroms) between the P atom of the flavin PO_4^{2-} group and the NH_2 group of Arg297 for all SsuD structures bound to a flavin substrate.

Table 2. Steady-State Kinetic Parameters of Wild-Type SsuD and Its Variants

	k_{cat} (min^{-1})	K_m (μM)	k_{cat}/K_m (μM^{-1} min^{-1})
SsuD	43.8 ± 4.3	31.2 ± 2.0	1.4 ± 0.2
E20A SsuD	36.3 ± 3.7	32.2 ± 4.6	1.1 ± 0.2
D111A SsuD	40.5 ± 3.8	36.3 ± 3.5	1.1 ± 0.2
R297A SsuD[a]	–[b]	–[b]	–[b]
R297K SsuD[a]	1.5 ± 0.1	35.2 ± 4.6	0.04 ± 0.01
R226A SsuD[a]	–[b]	–[b]	–[b]
R226K SsuD[a]	–[b]	–[b]	–[b]

[a]Previously reported results from refs 3 and 16. [b]No measurable activity detected.

interacting distances of 2–3 Å between Arg226 and OCS were found when $FMNH_2$ was also present in the active site (Figure 7). Desulfonation has been reported to occur through an ordered binding mechanism in which $FMNH_2$ must bind to SsuD first, followed by either octanesulfonate or O_2.[5] Accordingly, the simulations predicted a more organized active site in the presence of $FMNH_2$ with the cofactor anchored into the pocket by favorable hydrogen bonds provided by Tyr128 and Ser110 to the flavin phosphate oxygen atoms (Figure 8). Arg297 also provided electrostatic stabilization to the PO_4^{2-} group in $FMNH_2$ (Figure 5). Minimal movement occurred for OCS over 66% of the simulation when $FMNH_2$ was co-bound in the active site, compared to the more extensive motions found in its absence (Figure 7).

When SsuD was bound with the C4a-peroxyflavin intermediate, the simulations no longer found short interaction distances between Arg226 and OCS. Instead, the peroxy group of the $FMNOO^-$ was in the proximity of Arg226. Accordingly, for $FMNOO^-$-bound SsuD, average distances of 2–3 Å between the terminal O of the peroxy group and the NH_2 group of Arg226 were computed with some deviations over the course of the simulation (Figure 6A). The inclusion of OCS in the SsuD active site enhanced the interaction between $FMNOO^-$ and Arg226; i.e., the peroxy–NH_2 distance was found to occupy almost exclusive values of 2–3 Å over the entire trajectory (Figure 6B). In previous experimental studies, there was no catalytic activity observed when Arg226 was substituted with Ala or Lys, although the binding affinity for reduced flavin was unaffected (Table 2).[16] Additionally, there was no peroxyflavin identified in rapid reaction kinetic analyses with the Arg226 variants, suggesting the peroxyflavin was not effectively stabilized for reaction with the alkanesulfonate substrate. Experimental studies have determined that an arginine is often critical in Baeyer–Villiger flavin monooxygenases by stabilizing the peroxyflavin intermediate through electrostatic interactions.[22−24] Interestingly, the distance in the second most dominant cluster between the C4a position of the flavin ring and the C-1 position of the octanesulfonate was predicted to be 5.28 Å for SsuD co-bound to $FMNOO^-$ and OCS (Figure 9). As a point of comparison, the Baeyer–Villiger monooxygenase MtmOIV enzyme has an estimated distance of ~5.3 Å between the C-1 atom of the substrate premithramycin B and the C4a position of the flavin ring.[41] Other flavin-dependent enzymes, e.g., RebC, also have reported average distances of 4.5–5.5 Å between the substrate and flavin.[42] An electrostatic potential generated between the $FMNOO^-$ and OCS in SsuD finds an overlap of the two volumes that correlates nicely with the interaction distance necessary for nucleophilic attack (Figure 9).

The pH profile of k_{cat} for SsuD revealed two ionizable residues that are important for catalytic events.[16] One ionizable group had an upper pK_a value of 9.5 ± 0.1, suggesting that this group must be protonated for catalysis to occur. The k_{cat}–pH profile reflects the protonation state of groups necessary for catalysis to occur, including product release, and could represent the active site acid involved in the reprotonation of the $FMNO^-$ intermediate. These initial studies implicated Arg226 as the active site acid capable of donating a proton to the $FMNO^-$ intermediate for eventual product release (Scheme 2). Results from steady-state kinetic isotope effects further supported the role of Arg226 as the amino acid involved in proton donation that prompts a conformational change leading to solvation of the active site and eventual product release.[17]

dx.doi.org/10.1021/bi5002085 | Biochemistry 2014, 53, 3308–3317

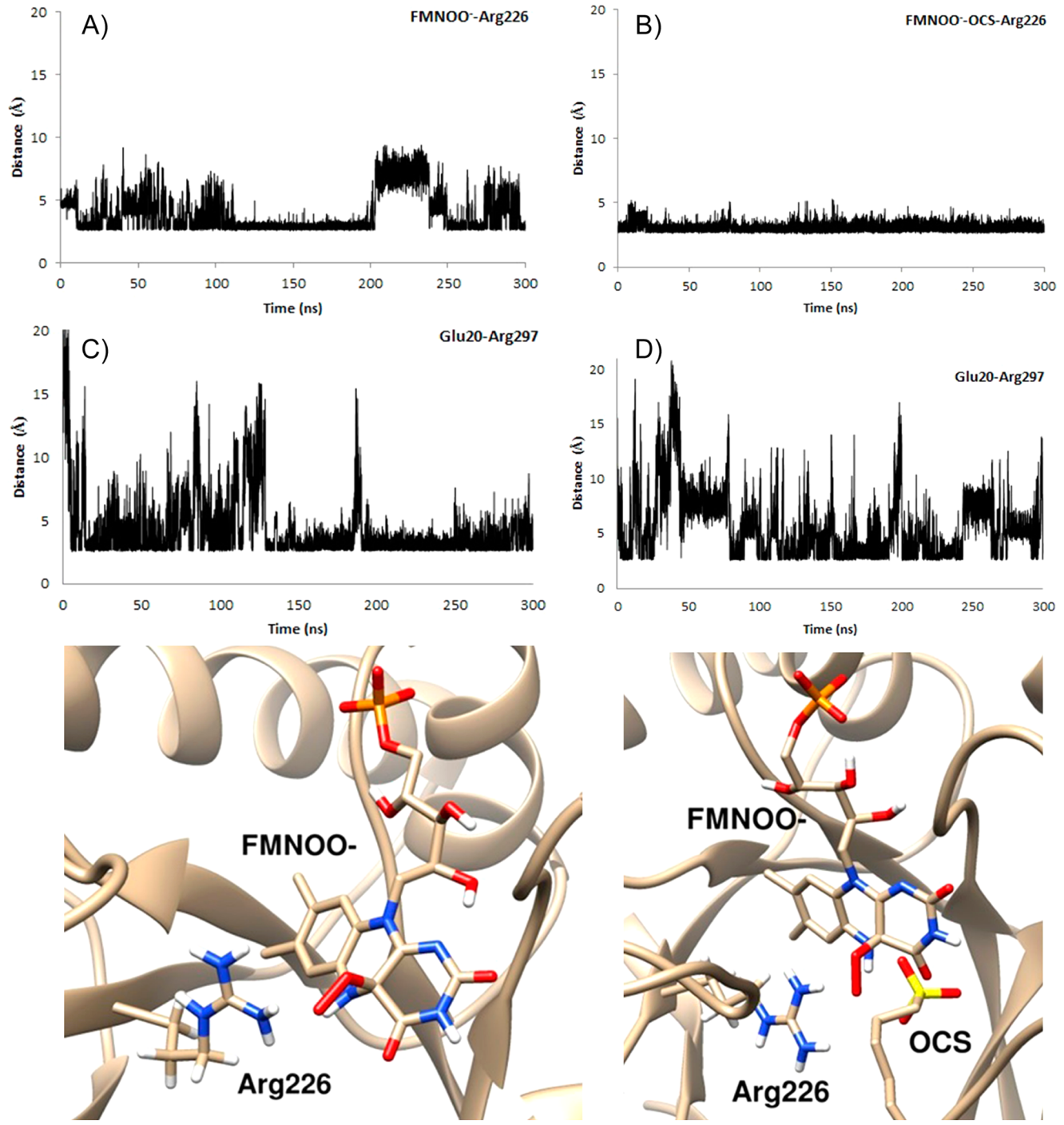

Figure 6. Distance calculations between the peroxy group of $FMNOO^-$ and the NH_2 group of Arg226 for the (A) $FMNOO^-$-bound SsuD and (B) $FMNOO^-$—OCS-bound SsuD systems. Distance calculations between Glu20 and Arg297 for the (C) $FMNOO^-$-bound SsuD and (D) $FMNOO^-$—OCS-bound SsuD systems. At the bottom are illustrated structures that are the dominant cluster from each $FMNOO^-$-bound and $FMNOO^-$—OCS-bound SsuD simulations.

The pK_a value appears to be at odds with arginine's typical free solution pK_a of 12.5; however, Cys54 has been proposed to help modify the pK_a of Arg226.[16] We did not investigate SsuD bound to $FMNO^-$, but distance calculations between Arg226 and Cys54 with $FMNOO^-$ and OCS co-bound in the active site can serve as a point of comparison. An average distance of 11.4 Å was computed between the two residues with a value of 8.5 Å at their closest point during the simulation (Figure S13 of the Supporting Information). As another point of comparison, the apo SsuD crystal structure (PDB entry 1M41) was used in conjunction with the pK_a prediction program PROPKA 3.1[43,44] to estimate the pK_a of Arg226 and Cys54. A computed pK_a value of 9.79 for Arg226 lends support to the idea of the residue acting as an active site acid as assigned in experimental studies, while Cys54 had a value of 10.68.

CONCLUSIONS

Molecular dynamics simulations were conducted for SsuD structures containing six different combinations of the $FMNH_2$, $FMNOO^-$, and OCS substrates according to the proposed

dx.doi.org/10.1021/bi5002085 | *Biochemistry* 2014, 53, 3308−3317

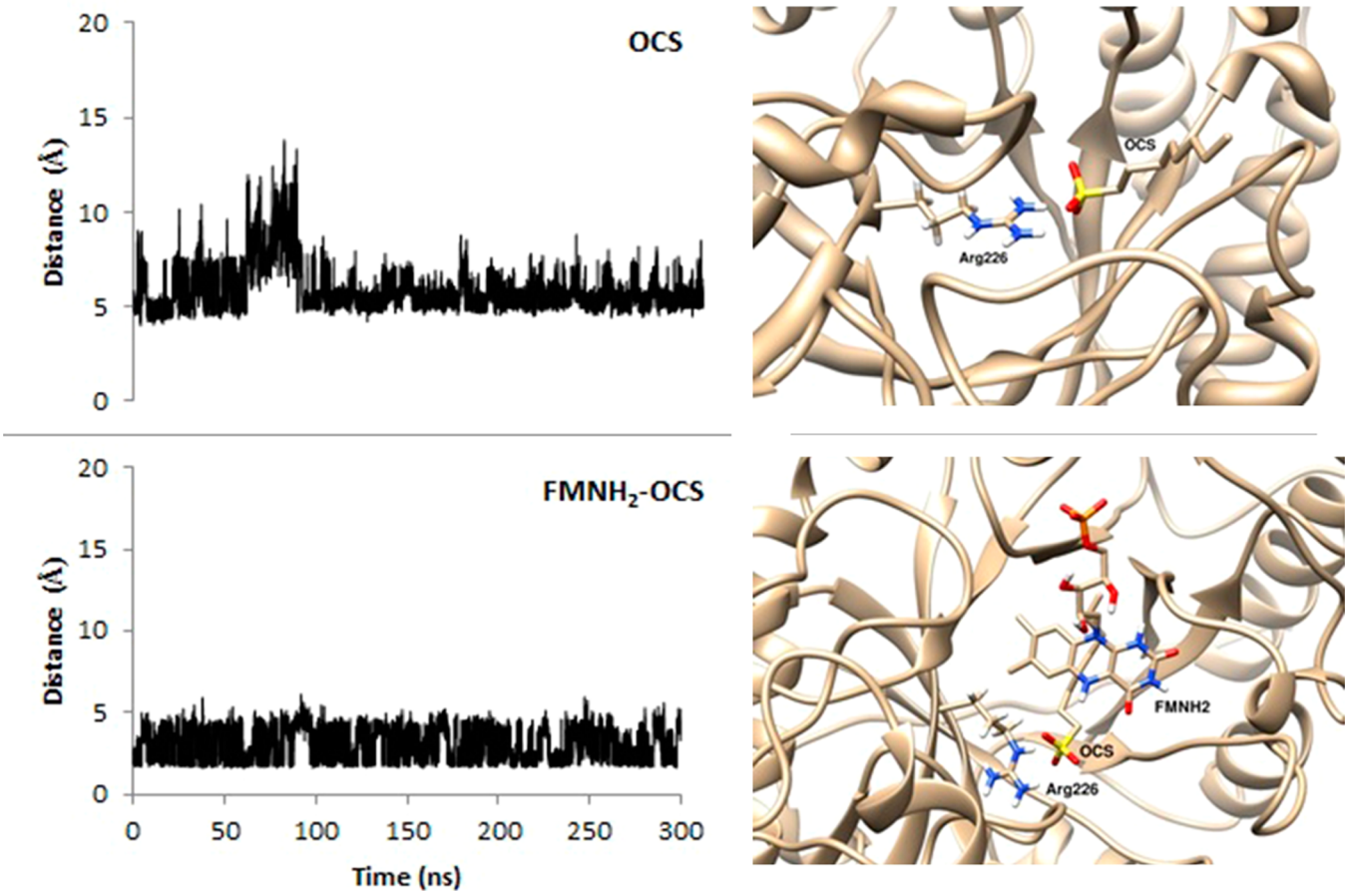

Figure 7. Distance calculations between the sulfur of OCS and the NH_2 group of Arg226 for the SsuD structures bound solely to OCS (top) and to both $FMNH_2$ and OCS (bottom), respectively. The dominant cluster structures for both enzymatic systems are illustrated.

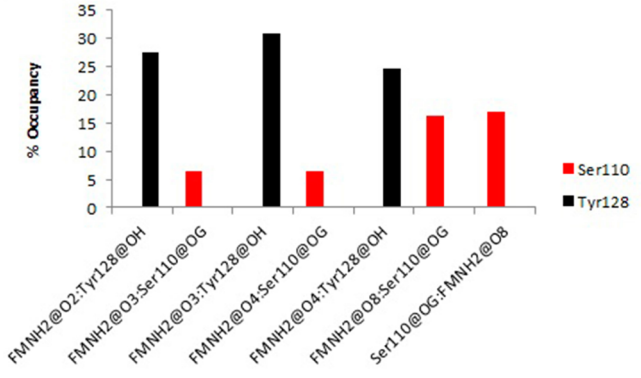

Figure 8. All hydrogen bond interactions (acceptor:donor) occupying >3% of the entire simulation for $FMNH_2$-bound SsuD.

Baeyer–Villiger mechanism given in Scheme 2. Detailed examination of the calculations has provided the following insight into the catalytic mechanism of SsuD.

(1) Octanesulfonate binds poorly to SsuD in the absence of flavin. No active site residues appear to adequately anchor the substrate into the active site; e.g., Arg226 is an average distance of 4–5 Å from the sulfonate group (Figure 7). Large and continual motions for OCS within the active site were computed.

(2) The binding of reduced flavin stabilized the motions associated with the active site (Figure 2). The reduced flavin is anchored into the binding pocket in the region encompassing residues 160–200 and is stabilized by a hydrogen bond network between the phosphate group of the cofactor and active site residues Tyr128, Ser110, and Arg297 (Figures 5 and 8). With both $FMNH_2$ and OCS bound to SsuD, Arg226 formed tight interaction average distances of 2–3 Å between the sulfonate group of OCS and the NH_2 group of the arginine (Figure 7). The calculations support experimental observations that SsuD binds $FMNH_2$ prior to OCS.[5]

(3) A salt bridge between Arg297 and Asp111 has been proposed to enforce a closed conformation as a method for blocking additional substrates and/or bulk solvent from entering the active site.[15] However, these simulations did not find the Arg297–Asp111 salt bridge to be dominant with <10% hydrogen bond occupancy when $FMNH_2$ was present (Figure 4). The alternative salt bridge between Arg297 and Glu20, or the open active site conformation, had ~5% hydrogen bond occupancy throughout the $FMNH_2$-bound simulation (Figure 4). Steady-state kinetic analyses and flavin binding experiments found k_{cat}/K_m and K_d values for the E20A and D111A SsuD variants that were similar to the wild-type SsuD values (Table 2). This suggests that the dynamic conformational switch to the active conformation does not exist or is not initiated by Arg297–Asp111 to Arg297–Glu20 salt bridges. Instead, the predicted role of Arg297 was to interact with the PO_4^{2-} group of reduced flavin (Figure 5).

(4) Binding of $FMNOO^-$ to the SsuD active site allowed a favorable interaction between the peroxyflavin group and the NH_2 group of Arg226 with average distances of 2–3 Å with

dx.doi.org/10.1021/bi5002085 | *Biochemistry* 2014, 53, 3308–3317

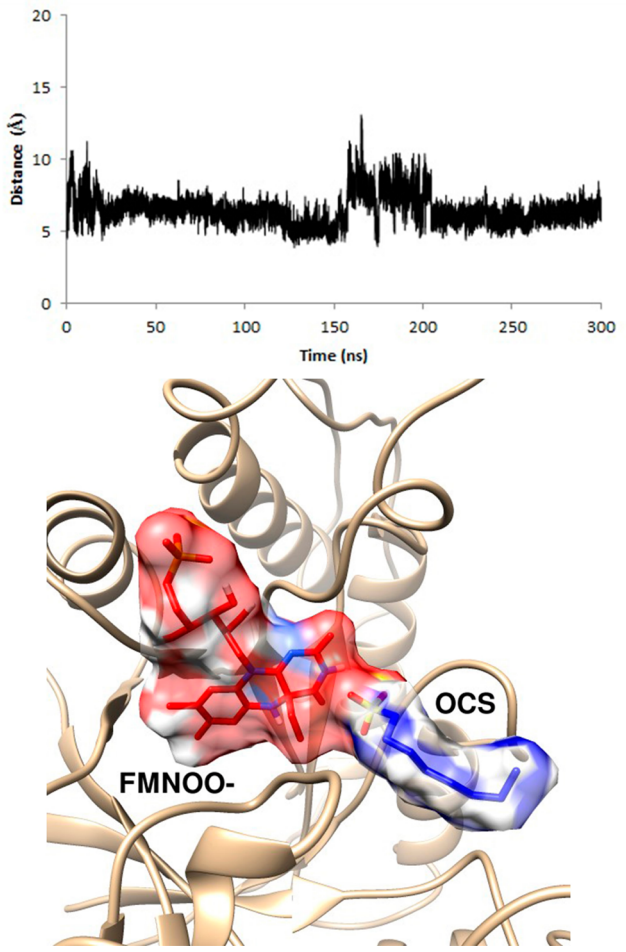

Figure 9. Distance calculation between the C4a ring position of the $FMNOO^-$ intermediate and the C-1 position of OCS and illustrated overlap of the electrostatic potential surfaces of the $FMNOO^-$ (red) and OCS (blue) in SsuD.

some deviations (Figure 6A). It may be postulated that Arg226 "protects" the peroxyflavin intermediate from solvent through electrostatic interactions. Accordingly, the experimental R226A and R226K SsuD variants possessed no detectable activity and no measurable formation of the C4a-(hydro)peroxyflavin intermediate.[16] Arg226 has also been experimentally proposed to be the active site acid participating in the protonation of the $FMNO^-$ intermediate in a Baeyer–Villiger mechanism (Scheme 2).[16] The computed pK_a for Arg226 also lends support for the residue acting as an active site acid.

(5) When both $FMNOO^-$ and OCS bind, the interaction distances between Arg226 and the peroxy group of $FMNOO^-$ rarely diverged from 2 to 3 Å, suggesting more significant protection of the peroxy group (Figure 6B). A predicted distance of 5.28 Å between the C4a position of the flavin ring and the C-1 position of the octanesulfonate is consistent with other monooxygenase systems and flavin-dependent enzymes that have reported average distances of 4.5–5.5 Å.[41,42] At this stage of the mechanism (Scheme 2), the active site appears to be well-suited for nucleophilic attack by the peroxyflavin intermediate upon the octanesulfonate (Figure 9).

(6) Examination of the mobile loop region (residues 250–282) over multiple simulations, including two separate 300 ns simulations of the SsuD system with $FMNOO^-$ OCS bound, found a highly active and flexible region, but no evidence of a lid gating conformational change [Figure 2, and see the movie of the overlaid apo (blue) and $FMNOO^-$–OCS-bound (red) SsuD systems given in the Supporting Information]. An MD simulation significantly longer than 300 ns or advanced sampling methods may be required to find such large structural changes. Alternatively, the mobile loop's primary function could be to mediate the transfer of $FMNH_2$ from SsuE to SsuD.[5,14]

■ ASSOCIATED CONTENT

Supporting Information

Tables of docking grid dimensions and percent occupancy for MD clusters, additional figures of SsuD clusters, absolute rmsf values for bound SsuD structures, distance calculations for the $FMNOO^-$–OCS-bound SsuD system, a table of GAFF parameters for substrates, the complete ref 33, and a movie of the apo and $FMNOO^-$–OCS-bound SsuD systems. This material is available free of charge via the Internet at http://pubs.acs.org.

■ AUTHOR INFORMATION

Corresponding Author

*E-mail: orlando.acevedo@auburn.edu. Phone: (334) 844-6549.

Funding

This work was supported by National Science Foundation Grant MCB-0545048 (to H.R.E.).

Notes

The authors declare no competing financial interest.

■ ACKNOWLEDGMENTS

Gratitude is expressed to the Alabama Supercomputer Center for support of this research.

■ ABBREVIATIONS

$FMNOO^-$, C4a-peroxyflavin intermediate; OCS, octanesulfonate; SsuE, alkanesulfonate flavin reductase; SsuD, alkanesulfonate monooxygenase.

■ REFERENCES

(1) Ellis, H. R. (2010) The FMN-dependent two-component monooxygenase systems. *Arch. Biochem. Biophys. 497*, 1–12.

(2) Ellis, H. R. (2011) Mechanism for sulfur acquisition by the alkanesulfonate monooxygenase system. *Bioorg. Chem. 39*, 178–184.

(3) Carpenter, R. A., Xiong, J., Robbins, J. M., and Ellis, H. R. (2011) Functional role of a conserved arginine residue located on a mobile loop of alkanesulfonate monooxygenase. *Biochemistry 50*, 6469–6477.

(4) Carpenter, R. A., Zhan, X., and Ellis, H. R. (2010) Catalytic role of a conserved cysteine residue in the desulfonation reaction by the alkanesulfonate monooxygenase enzyme. *Biochim. Biophys. Acta 1804*, 97–105.

(5) Zhan, X., Carpenter, R. A., and Ellis, H. R. (2008) Catalytic importance of the substrate binding order for the $FMNH_2$-dependent alkanesulfonate monooxygenase enzyme. *Biochemistry 47*, 2221–2230.

(6) Gao, B., and Ellis, H. R. (2007) Mechanism of flavin reduction in the alkanesulfonate monooxygenase system. *Biochim. Biophys. Acta 1774*, 359–367.

(7) Eichhorn, E., Davey, C. A., Sargent, D. F., Leisinger, T., and Richmond, T. J. (2002) Crystal structure of *Escherichia coli* alkanesulfonate monooxygenase SsuD. *J. Mol. Biol. 324*, 457–468.

(8) Eichhorn, E., van der Ploeg, J. R., and Leisinger, T. (1999) Characterization of a two-component alkanesulfonate monooxygenase from *Escherichia coli*. *J. Biol. Chem. 274*, 26639–26646.

(9) Abdurachim, K., and Ellis, H. R. (2006) Detection of protein-protein interactions in the alkanesulfonate monooxygenase system from *Escherichia coli*. *J. Bacteriol. 188*, 8153−8159.
(10) Gao, B., and Ellis, H. R. (2005) Altered mechanism of the alkanesulfonate FMN reductase with the monooxygenase enzyme. *Biochem. Biophys. Res. Commun. 331*, 1137−1145.
(11) Fisher, A. J., Raushel, F. M., Baldwin, T. O., and Rayment, I. (1995) Three-dimensional structure of bacterial luciferase from *Vibrio harveyi* at 2.4 Å resolution. *Biochemistry 34*, 6581−6586.
(12) Li, L., Liu, X., Yang, W., Xu, F., Wang, W., Feng, L., Bartlam, M., Wang, L., and Rao, Z. (2008) Crystal structure of long-chain alkane monooxygenase (LadA) in complex with coenzyme FMN: Unveiling the long-chain alkane hydroxylase. *J. Mol. Biol. 376*, 453−465.
(13) Xiong, J., and Ellis, H. R. (2012) Deletional studies to investigate the functional role of a dynamic loop region of alkanesulfonate monooxygenase. *Biochim. Biophys. Acta 1824*, 898−906.
(14) Malabanan, M. M., Amyes, T. L., and Richard, J. P. (2010) A role for flexible loops in enzyme catalysis. *Curr. Opin. Struct. Biol. 20*, 702−710.
(15) Ferrario, V., Braiuca, P., Tessaro, P., Knapic, L., Gruber, C., Pleiss, J., Ebert, C., Eichhorn, E., and Gardossi, L. (2012) Elucidating the structural and conformational factors responsible for the activity and substrate specificity of alkanesulfonate monooxygenase. *J. Biomol. Struct. Dyn. 30*, 74−88.
(16) Robbins, J. M., and Ellis, H. R. (2012) Identification of critical steps governing the two-component alkanesulfonate monooxygenase catalytic mechanism. *Biochemistry 51*, 6378−6387.
(17) Robbins, J. M., and Ellis, H. R. (2014) Steady-State Kinetic Isotope Effects Support a Complex Role of Arg226 in the Proposed Desulfonation Mechanism of Alkanesulfonate Monooxygenase. *Biochemistry 53*, 161−168.
(18) Fisher, A. J., Thompson, T. B., Thoden, J. B., Baldwin, T. O., and Rayment, I. (1996) The 1.5-Å resolution crystal structure of bacterial luciferase in low salt conditions. *J. Biol. Chem. 271*, 21956−21968.
(19) Campbell, Z. T., Weichsel, A., Montfort, W. R., and Baldwin, T. O. (2009) Crystal structure of the bacterial luciferase/flavin complex provides insight into the function of the β subunit. *Biochemistry 48*, 6085−6094.
(20) Xin, X., Xi, L., and Tu, S. C. (1991) Functional consequences of site-directed mutation of conserved histidyl residues of the bacterial luciferase α subunit. *Biochemistry 30*, 11255−11262.
(21) Huang, S., and Tu, S. C. (1997) Identification and characterization of a catalytic base in bacterial luciferase by chemical rescue of a dark mutant. *Biochemistry 36*, 14609−14615.
(22) Palfey, B. A., and McDonald, C. A. (2010) Control of catalysis in flavin-dependent monooxygenases. *Arch. Biochem. Biophys. 493*, 26−36.
(23) Orru, R., Dudek, H. M., Martinoli, C., Pazmiño, D. E., Royant, A., Weik, M., Fraaije, M. W., and Mattevi, A. (2011) Snapshots of enzymatic Baeyer-Villiger catalysis: Oxygen activation and intermediate stabilization. *J. Biol. Chem. 286*, 29284−29291.
(24) Malito, E., Alfieri, A., Fraaije, M. W., and Mattevi, A. (2004) Crystal structure of a Baeyer-Villiger monooxygenase. *Proc. Natl. Acad. Sci. U.S.A. 101*, 13157−13162.
(25) Eswar, N., Marti-Renom, A., Webb, B., Madhusudhan, M. S., Eramian, D., Shen, M., Pieper, U., and Sali, A. (2006) Comparative Protein Structure Modeling with MODELLER. In *Current Protocols in Bioinformatics*, pp 5.6.1−5.6.30, John Wiley & Sons, Inc, New York.
(26) Trott, O., and Olson, A. J. (2010) AutoDock Vina: Improving the Speed and Accuracy of Docking with a New Scoring Function, Efficient Optimization and Multithreading. *J. Comput. Chem. 31*, 455−461.
(27) Case, D. A., Darden, T. A., Cheatham, T. E., III, Simmerling, C. L., Wang, J., Duke, R. E., Luo, R., Walker, R. C., Zhang, W., Merz, K. M., Roberts, B., Hayik, S., Roitberg, A., Seabra, G., Swails, J., Götz, A. W., Kolossváry, I., Wong, K. F., Paesani, F., Vanicek, J., Wolf, R. M., Liu, J., Wu, X., Brozell, S. R., Steinbrecher, T., Gohlke, H., Cai, Q., Ye, X., Wang, J., Hsieh, M. J., Cui, G., Roe, D. R., Mathews, D. H., Seetin, M. G., Salomon-Ferrer, R., Sagui, C., Babin, V., Luchko, T., Gusarov, S., Kovalenko, A., and Kollman, P. A. (2012) *AMBER 12*, University of California, San Francisco.
(28) Jorgensen, W. L., Chandrasekhar, J., Madura, J. D., Impey, W., and Klein, M. L. (1983) Comparison of simple potential functions for simulating liquid water. *J. Chem. Phys. 79*, 926−935.
(29) Hornak, V., Abel, R., Okur, A., Strockbine, B., Roitberg, A., and Simmerling, C. (2006) Comparison of Multiple Amber Force Fields and Development of Improved Protein Backbone Parameters. *Proteins: Struct., Funct., Bioinf. 65*, 712−725.
(30) Wang, J., Wolf, R. M., Caldwell, J. W., Kollman, P. A., and Case, D. A. (2004) Development and Testing of a General Amber Force Field. *J. Comput. Chem. 25*, 1157−1174.
(31) Jorgensen, W. L. (1998) BOSS: Biochemical and Organic Simulation System. In *Encyclopedia of Computational Chemistry* (Schleyer, R., Ed.) pp 3281−3285, John Wiley & Sons Ltd., Athens, GA.
(32) Jorgensen, W. L., Maxwell, D. S., and Tirado-Rives, J. (1996) Development and testing of the OPLS all-atom force field on conformational energetics and properties of organic liquids. *J. Am. Chem. Soc. 118*, 11225−11236.
(33) Frisch, M. J., et al. (2009) *Gaussian 09*, revision B.01, Gaussian, Inc., Wallingford, CT.
(34) Goetz, A. W., Williamson, M. J., Xu, D., Poole, D., Le Grand, S., and Walker, R. C. (2012) Routine Microsecond Molecular Dynamics Simulations wither AMBER. Part I: Generalized Born. *J. Chem. Theory Comput. 8*, 1542−1555.
(35) Darden, T., York, D., and Pedersen, L. (1993) Particle Mesh Ewald: An N-log(N) Method for Ewald Sums in Large Systems. *J. Chem. Phys. 98*, 10089−10092.
(36) Humphrey, W., Dalke, A., and Schulten, K. (1996) VMD: Visual Molecular Dynamics. *J. Mol. Graphics 14*, 33−38.
(37) Roe, D. R., and Cheatham, T. E., III (2013) PTRAJ and CPPTRAJ: Software for Processing and Analysis of Molecular Dynamics Trajectory Data. *J. Chem. Theory Comput. 9*, 3084−3095.
(38) Shao, J., Tanner, S. W., Thompson, N., and Cheatham, T. E., III (2007) Clustering Molecular Dynamics Trajectories: 1. Characterizing the Performance of Different Clustering Algorithms. *J. Chem. Theory Comput. 3*, 2312−2334.
(39) Pettersen, E. F., Goddard, T. D., Huang, C. C., Couch, G. S., Greenblatt, D. M., Meng, E. C., and Ferrin, T. E. (2004) UCSF Chimera: A Visualization System for Exploratory Research and Analysis. *J. Comput. Chem. 25*, 1605−1612.
(40) Louie, T. M., Xie, X. S., and Xun, L. (2003) Coordinated production and utilization of $FADH_2$ by NAD(P)H-flavin oxidoreductase and 4-hydroxyphenylacetate 3-monooxygenase. *Biochemistry 42*, 7509−7517.
(41) Beam, M. P., Bosserman, M. A., Noinaj, N., Wenhenkel, M., and Rohr, J. (2009) Crystal Structure of Baeyer-Villiger Monooxygenase MtmOIV, the Key Enzyme of the Mithramycin Biosynthetic Pathway. *Biochemistry 48*, 4476−4487.
(42) Ryan, K. S., Howard-Jones, A. R., Hamill, M. J., Elliott, S. J., Walsh, C. T., and Drennan, C. L. (2007) Crystallographic trapping in the rebeccamycin biosynthetic enzyme RebC. *Proc. Natl. Acad. Sci. U.S.A. 104*, 15311−15316.
(43) Olsson, M. H. M., Søndergard, C. R., Rostkowski, M., and Jensen, J. H. (2011) PROPKA3: Consistent Treatment of Internal and Surface Residues in Empirical pKa predictions. *J. Chem. Theory Comput. 7*, 525−537.
(44) Søndergaard, C. R., Olsson, M. H. M., Rostkowski, M., and Jensen, J. H. (2011) Improved Treatment of Ligands and Coupling Effects in Empirical Calculation and Rationalization of pKa Values. *J. Chem. Theory Comput. 7*, 2284−2295.